MoDE: Mixture-of-Decision-Experts for DRL in High-Dimensional Coupled Wireless Optimization

Shiyi Lin, Hongyang Du

Abstract—Next-generation wireless networks must deliver ultra reliable connectivity, extreme data rates, and low latency for applications such as immersive communications and intelligent transportation. Achieving these targets is challenging because design variables across multiple layers are tightly coupled, which gives rise to high-dimensional, nonconvex optimization problems that are difficult to solve efficiently in real time. Existing approaches, whether classical model-based optimization or generic learning-based methods, struggle to balance computational efficiency, stability, and scalability in such settings. To address this challenge and enhance system performance, we propose a novel learning-based framework which integrates Mixture-of-Decision-Experts (MoDE) with Deep Reinforcement Learning (DRL). The MoDE, leveraging adaptive routing and heterogeneous expert allocation, effectively decomposes complex wireless control tasks into structured subtasks for specialized processing. We evaluate the proposed architecture against a heuristic baseline with low inference complexity and a conventional Multilayer Perceptron (MLP)-based DRL approach. Numerical results show that our method outperforms both standard MLP-based DRL and heuristic baselines in terms of convergence speed and overall performance; furthermore, allocating more experts to higher-dimensional decision layers yields additional gains over uniform-expert-allocations design, demonstrating both efficiency and robustness.

Index Terms—Generative AI (GAI), Wireless Networks, Deep Reinforcement learning (DRL), Mixture of Experts (MoE)

1 Introduction

Recently, the relentless growth of wireless applications, from immersive extended-reality services to intelligent transportation, have been driving the evolution toward Sixth-Generation (6G) networks. These systems aim to deliver ubiquitous connectivity, extreme data rates, and low-latency services under dense device deployments [1], [2]. To meet these demands, emerging infrastructures are becoming increasingly heterogeneous and ultra-dense [3], incorporating not only many base stations [4] but also new components such as Reconfigurable Intelligent Surfaces (RIS) [5], Unmanned Aerial Vehicles (UAVs) [6], and edge computing nodes [7]. This architectural shift, combined with its capacity to support massive device connectivity while guaranteeing diverse levels of Quality-of-Service (QoS) [8], [9], unlocks superior performance metrics like enhanced spectral and energy efficiency together with low latency [2], [10]. This collective progress is reshaping physical layer design toward new operating paradigms.

The same innovations that enable richer services also introduce hard optimization challenges. The growing system scale and component heterogeneity significantly increase the dimensionality and nonlinearity of system models [11], [12], thereby turning classical design tasks into large-scale, high-dimensional, and nonconvex optimization problems [13], [14]. These challenges manifest as tightly coupled decision problems. For example, antenna placement, beamforming and power allocation interacting through the physical channel and receiver processing across many wireless applications, where the optimization of one component strongly affects others [15]. Meanwhile, practical deployments further demand real-time or near real-time solutions, imposing severe computational pressure and requiring algorithms that deliver high-quality joint decisions within tight latency budgets [16], [17].

Prior work has pursued model-based and learning-based approaches. For near-field beam training, the authors in [18] propose a two-dimensional, multi-resolution hierarchical beam-training framework that designs polar-domain codebooks and applies a coarse-to-fine search to reduce overhead in antenna positioning and beam alignment; however, the scheme depends on precomputed multi-resolution codebooks and still requires exhaustive sampling of angle–distance grid points within each codebook level, which limits adaptability in highly dynamic mobile settings. An alternative model-based line uses Fractional-Programming (FP) and Block-Coordinate updates to transform multiple-ratio problems into iterative convex subproblems with provable convergence to stationary points [19]. Its matrix extension, e.g., the FPLinQ approach proposed in [20], further enables joint scheduling, power allocation and multi-stream beamforming and shows strong sum-rate performance in dense Device-to-Device/MIMO settings; nevertheless, these methods rely on iterative subproblem solves, grid/combinatorial searches for discrete choices, and can be sensitive to initialization and per-iteration cost in large-scale deployments. Hence, such methods may struggle to meet real-time adaptation requirements in large-scale, high-dimensional, and heterogeneous deployments. As for learning-based approaches, DRL circumvent explicit modeling by learning policies from interaction and therefore have been applied to many non-convex and coupled optimization in wireless network such as beam management, UAVs relay

and vehicular settings [21]–[23]. For example, authors in [22] develop a DRL algorithm for joint beamforming, power control and interference coordination in cellular settings and demonstrate notable Signal-to-Interference-plus-Noise Ratio (SINR) and Spectral Efficiency (SE) gains versus both the tabular Q-learning algorithm and the fixed power allocation algorithm. However, DRL exhibits its own limitations, where many of its methods are sample-inefficient, struggle with very large action spaces, and exhibit unstable training when the control problem decomposes into multiple interacting subtasks. This contrast highlights a clear gap, that is, neither purely model-based nor vanilla end-to-end learning fully balances scalability, data efficiency, specialization across subtasks, and stable training in tightly coupled wireless control problems. Taken together, these limitations motivate the following research question:

- *How can we obtain data-efficient, scalable policies that solve deeply coupled wireless optimization problems while avoiding interference between heterogeneous subtasks?*

Addressing this question calls for architectures capable of decomposing complex decisions into specialized subtasks [24], [25], thereby increasing representational capacity in a controlled way while maintaining stable learning throughout continuous, multimodal control. Mixture-of-experts (MoE) architectures are a natural candidate because they distribute capacity across specialized experts via learned routing, which reduces cross-task interference and enables more focused representation learning [26], [27]. Recent work in the Large Language Model (LLM) has explored dense activation or dense training variants of MoE as a practical way to stabilize expert initialization and encourage richer expert specialization before committing to sparse routing [28], [29]. Dense activation strategies that route to many or all experts improve specialization and reduce routing overlap at the cost of increased computation per example. This trade-off, higher compute for stronger specialization and more robust learning, matches our goal of solving tightly-coupled wireless optimization tasks where representational fidelity and stable training matter.

To satisfy the requirements above, we propose a MoDE driven decision aided DRL framework tailored for tightly-coupled wireless optimization problems existing in multiple application domains. Specifically, MoDE has three design characteristics:

- Task decomposition [27]. The MoDE-based actor network is organized in layers that reflect natural groupings of the joint action such as position selection, power allocation, and beamforming decoding. Each layer produces the layer-specific action component and is modeled by its own MoDE block, which reduces the dimensionality and cross-talk facing any single module and clarifies learning targets for experts.
- Expert specialization [30]. Rather than uniformly assigning the same number of experts to every layer, MoDE allows heterogeneous expert counts and internal segmentation, where high-dimensional or more complex layers receive more experts while simpler layers use fewer. We also design shared experts across layers to capture common structure. This allocation improves representational fidelity and stabilizes learning in composite action spaces.
- Adaptive routing [31] and dense activation. MoDE allows routing policies to activate multiple experts when subtasks interact strongly, trading extra computation for improved representational fidelity and stable learning.

Algorithmically, MoDE is unified and agnostic to deployment. The training loop is end-to-end and implemented with an off-policy, entropy-regularized backbone so that continuous, multimodal control benefits from robust exploration and sample reuse. At deployment time, MoDE is flexible because it can run entirely on a single platform or be partitioned across devices.

To demonstrate the practical relevance and generality of MoDE, we evaluate it on three representative classes of tightly-coupled wireless control problems: (i) the optimization of Pinching Antenna Systems (PASS) requiring joint position and beamforming design optimization; (ii) Multi-User Multiple-Input Multiple-Output (MU-MIMO), where power allocation and beamforming design are jointly optimized; and (iii) joint transmission and reflection optimization in a RIS-aided MIMO system. Although these scenarios rely on different physical mechanisms, including reconfigurable antenna geometry, spatial multiplexing at arrays, and environment shaping via metasurfaces, they all produce the same kind of multivariable, tightly-coupled decision structure, yielding high-dimensional, nonconvex joint optimization objectives [11], [13]. It is precisely this class of structured, high-dimensional problems that the MoDE framework is designed to address. The main contributions of this paper are summarized as follows.

- We propose the MoDE, a general-purpose MoE that can be readily integrated into various RL frameworks for structured decision making. MoDE factorizes tightly-coupled, high-dimensional, and strongly nonconvex optimization problems into staged expert modules, and supports heterogeneous expert allocation, fine-grained expert segmentation and shared experts, enabling targeted specialization across decisions.
- We realize the decision-making idea within a DRL framework by integrating MoDE with Soft Actor-Critic (SAC) algorithm. We further provide concrete, scenario-specific algorithmic instantiations for three representative wireless problems in PASS, MU–MIMO, and RIS-aided MIMO cases.
- We perform many experiments that validate effectiveness of MoDE. Compared to a heuristic baseline and standard MLP-based RL, MoDE attains better system performance and faster convergence after sufficient training in our testbed scenarios. We also show that allocating more experts to higher-dimensional layers yields additional gains over uniform expert allocation.

2 Related work

In this section, we provide a brief review of three tightly-coupled wireless optimization scenarios including PASS,

MU-MIMO, and RIS-aided MIMO to clarify the concrete technical challenges that motivate MoDE.

2.1 Pinching Antenna Positions and Beamforming Design in PASS.

PASS have gained significant attention as a promising technology for enhancing system performance through reconfigurable antenna geometry, where discrete pinching elements attached to dielectric waveguides dynamically alter the physical geometry of the radiating aperture [32]. Recent work studies their use for downlink multiuser MIMO and shows that Activating different pinching elements dynamically modifies propagation paths and Line-of-Sight (LoS) components, thereby altering per-stream channel gains and phase alignments [33], [34], while adapting the transmit beamforming design further shapes the radiated waveforms to coherently combine signals from the activated Pinching Antennas (PAs) and optimize their alignment with these physically reconfigured channel characteristics. In other words, the placement of pinching elements and the digital beamformer jointly determine the baseband-equivalent channel matrix entries, including their phases [35], meaning a beamformer that provides coherent combining and high array gain for one antenna configuration may suffer phase misalignment or reduced gain under another configuration. This interdependence creates a tightly-coupled optimization landscape where the joint design problem becomes inherently high-dimensional and nonconvex, as antenna positions and beamforming coefficients must be co-optimized under continuous search spaces and physical constraints. These challenges underscore the need for architectures that can decompose such coupled decisions while maintaining representational fidelity across heterogeneous subtasks.

2.2 Power Allocation and Beamforming in MU-MIMO.

MU-MIMO, recognized as a cornerstone of modern wireless networks, has become increasingly essential for supporting high-capacity multi-user communications. In MU-MIMO, system performance is critically shaped by the interplay between transmit power allocation and beamforming design, since they collectively control the trade-off between sum-rate, fairness, and energy efficiency [36], [37]. Adjusting the power assigned to a stream directly changes the received signal strengths and alters the interference experienced by other users [38], while modifying beamforming vectors changes the spatial distribution of radiated energy and thus reshapes per-user channel gains and interference geometry [39], [40]. This mutual dependency leads to a strongly coupled and nonconvex optimization problem, as changes in one domain alter the optimal solution in the other. Many practical algorithms such as Weighted Minimum Mean-Square Error (WMMSE) and alternating optimization therefore treat beamforming and power jointly, but the resulting joint objective typically admits many stationary points [19]. Although these methods could converge to stationary points, they can be slow or sensitive to initialization in very high-dimensional regimes. Moreover, such iterative approaches face real-time applicability challenges in high-dimensional regimes due to their computational latency. These properties, high action dimensionality, strong cross-term coupling, and multiple local optima, make MU-MIMO an archetypal tightly-coupled problem requiring specialized decomposition approaches.

2.3 RIS Phase and Beamforming Design in RIS-aided MIMO.

RIS-aided MIMO systems have emerged as a transformative technology for dynamic environment shaping in next-generation wireless networks, particularly in enhancing coverage and SE through joint active and passive beamforming [5]. The configuration of RIS phase shifts and transmit beamforming collectively shapes the end-to-end channel response, where tuning RIS phases applies multiplicative adjustments to reflected paths while adapting beamforming alters spatial excitation and signal combining. On one hand, tuning the RIS phase shifts modifies the composite channel response by applying a multiplicative effect to signals along reflected paths. On the other hand, adapting the transmit beamforming alters the spatial excitation of the propagation environment, influencing how signals combine after reflection [41], [42]. Due to the fact that RIS phases and transmitter beamforming interact multiplicatively and that RIS elements have unit modulus constraints, changes on one side change the best choice on the other and the joint problem is strongly coupled and nonconvex [43], [44]. This mathematical structure makes achieving global optima difficult with conventional methods, i.e., Alternating Minimization (AL), often struggle to attain global optima under real-time requirements in dynamic channel conditions, due to high computational complexity and sensitivity to initial points [45]. The inherent coupling between RIS phase shifts and continuous beamforming parameters highlights the demand for architectures that enable robust coordination between active and passive components under stringent latency constraints.

3 MoDE-aided SAC

In this section, we propose the MoDE-aided SAC method. Specifically, we first discuss the MoDE architecture, and then we explain the SAC feedback framework that utilizes SE as the reward signal for policy optimization. We also provide a theoretical complexity analysis.

3.1 MoDE-Based Actor Network Architecture

Our policy network is a two-stage MoDE that jointly predicts a configuration action and a high-dimensional signal action. As shown in Fig. 1, the MoDE-based actor network consists of:

3.1.1 Layered MoDE Architecture with Heterogeneous Expert Allocation

In a conventional MoE actor, all experts receive the same state input and are jointly trained to output actions for a single decision step. However, direct application creates two main issues in the application of high-dimensional coupled wireless optimization:

- Coupled learning difficulty. Structural/configuration decisions and signal-level actions require different

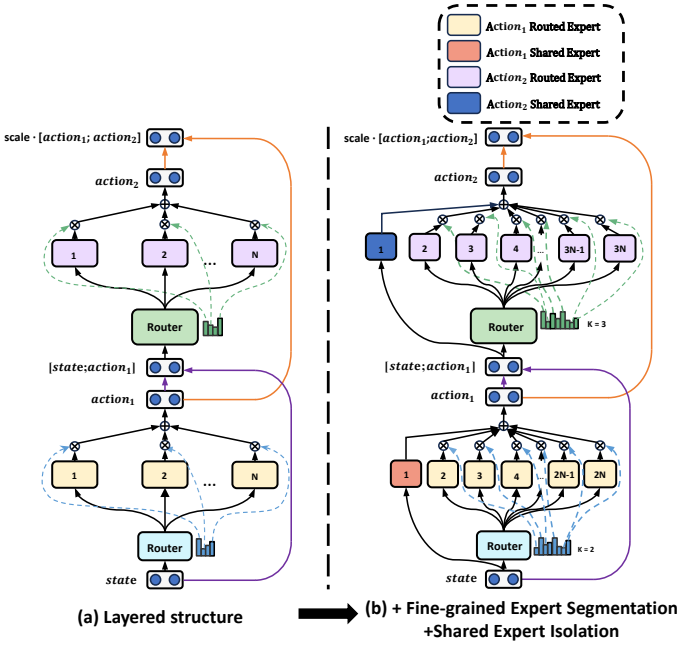

Fig. 1: Illustration of general MoDE. Subfigure (a) showcases the layered MoDE structure. Subfigure (b) illustrates the fine-grained expert segmentation strategy and the integration of the shared expert isolation strategy.

feature sensitivities and inductive biases. Training a single-layer MoE to handle both kinds of outputs induces noisy gradient updates and routing conflicts as configuration-related gradients interfere with signal-level specialization.

- Slow convergence and exploration cost. When the action space is large and multi-stage, the MoDE router simultaneously learn to route inputs for both tasks, which increases exploration cost and delays expert specialization.

If we separate the decision process into multiple MoDE layers, each layer can specialize in its own subtask. This "layered" design transforms the learning problem from one large entangled decision into two simpler sequential decisions. This hierarchical decomposition maintains the computational efficiency of standard MoDE and achieving higher specialization without interference from unrelated subtasks. In pursuit of the goal, we design the Layered MoDE-based actor network consisting of two sequential MoDE stages:

- Configuration MoDE layer: Routes the state to configuration experts, producing a structural/configuration action.
- Signal MoDE layer: Takes both the state and the chosen configuration as input, which we express as an enriched state

$$\tilde{s} = [s; a] \in \mathbb{R}^{d_{\text{state}}+d_{\text{config}}}, \tag{1}$$

where a denotes the intermediate configuration action and d_{config} represents its dimensionality. Then we can rout the enriched state $\tilde{s}$ to experts in the signal MoDE layer for the final optimization.

Crucially, we assign different numbers of experts to the two MoDE layers. The configuration output is typically correspondingly low and its mapping from state to antenna coordinates is relatively simple, while the signal mapping is high dimensional and highly nonlinear. Allocating more experts and finer grained segmentation to the signal layer increases representational capacity where it is most needed and enables distinct experts to specialize on diverse channel configurations. At the same time, assigning a smaller expert set to the configuration layer avoids unnecessary overparameterization and reduces routing overhead for the simpler subtask.

3.1.2 Fine-Grained Expert Segmentation and Shared Experts Isolation

In conventional MoDE with limited experts, a single expert often has to capture highly diverse patterns of knowledge. This forces the expert parameters to capture incompatible patterns, reducing their ability to optimize for any one pattern [27]. To address this, one strategy is to split an expert into smaller subexperts and activate more of them simultaneously. In this way, diverse knowledge can be distributed across specialized subspaces, allowing each subexpert to focus on a narrower scope of representation learning [30], [46].

However, diversity alone is not sufficient. In many routing strategies, different experts inadvertently learn overlapping common knowledge, leading to redundancy and inefficient parameter utilization. This overlap reduces the capacity available for capturing unique, specialized features. To mitigate this, we introduce dedicated shared experts that always receive input. These shared experts act as repositories of common knowledge, thereby freeing the fine-grained experts to focus exclusively on specialized features [46]. Together, segmentation and isolation create a complementary mechanism, segmentation enhances specialization, while shared experts centralize generalization.

Building on the Layered MoDE-based actor network architecture described above, we implement two categories of experts, configuration experts and signal experts. Each category contains fine-grained experts and one shared expert. Every expert is parameterized as a two-hidden-layer fully connected network with separate output heads for the mean and log standard deviation of a Gaussian distribution. The feedforward computation can be expressed as:

$$h_1 = \text{ReLU}(W_1 x + b_1), \quad W_1 \in \mathbb{R}^{d_h \times d_{\text{in}}}, \tag{2}$$

$$h_2 = \text{ReLU}(W_2 h_1 + b_2), \quad W_2 \in \mathbb{R}^{d_h \times d_h}, \tag{3}$$

$$\mu = W_\mu h_2 + b_\mu, \quad W_\mu \in \mathbb{R}^{d_{\text{out}} \times d_h}, \tag{4}$$

$$log\sigma = W_\sigma h_2 + b_\sigma, \quad W_\sigma \in \mathbb{R}^{d_{\text{out}} \times d_h}, \tag{5}$$

where $x \in \mathbb{R}^{d_{\text{in}}}$ is the input feature vector, d_{in} is the input dimension, d_h is the hidden dimension, and d_{out} is the output dimension. The parameters $W_1, W_2, W_\mu, W_\sigma$ are trainable weight matrices, and $b_1, b_2, b_\mu, b_\sigma$ are their associated bias vectors. The outputs $\mu \in \mathbb{R}^{d_{\text{out}}}$ and $\log \sigma \in \mathbb{R}^{d_{\text{out}}}$ represent the mean and log standard deviation of the Gaussian distribution, respectively.

The output of one expert feedforward network is

$$\text{ExpertFFN}(x) = (\mu, \log \sigma).$$

Hence, Fine-Grained Experts outputs and Shared expert outputs can be expressed as:

$$(\mu_i^{\text{config}}, \log \sigma_i^{\text{config}}) = E_i^{\text{config}}(s), \quad i = 1 \dots n, \tag{6}$$

$$(\mu_j^{\text{signal}}, \log \sigma_j^{\text{signal}}) = E_j^{\text{signal}}(\tilde{s}), \quad j = 1 \dots m, \tag{7}$$

$$(\mu_k^{\text{config}}, \log \sigma_k^{\text{config}}) = E_k^{\text{config}}(s), \tag{8}$$

$$(\mu_k^{\text{signal}}, \log \sigma_k^{\text{signal}}) = E_k^{\text{signal}}(\tilde{s}), \tag{9}$$

where n and m denote the segmentation factors for the configuration and signal experts, respectively. Specifically, each configuration expert FFN is split into n sub-experts by reducing the hidden dimension of each FFN to $\frac{1}{n}$ of its original size. To maintain constant computational cost, the number of simultaneously activated sub-experts is increased to n times the original. An analogous segmentation is applied to the signal experts with factor m.
Each MoDE layer employs a lightweight router that maps the layer input x to per-expert gating logits. The logits are converted to a normalized weight vector by a softmax as

$$\mathbf{w} = \frac{\exp((R\mathbf{x} + \mathbf{r})_i)}{\sum_{j=1}^{E} \exp((R\mathbf{x} + \mathbf{r})_j)} \in \mathbb{R}^E,$$

where $R \in \mathbb{R}^{E \times d_{\text{in}}}$ and $\mathbf{r} \in \mathbb{R}^E$ are the router parameters, d_{in} is the input dimension, and E is the number of fine-grained experts in that layer. The resulting weights satisfy $w_i \geq 0$ and $\sum_{i=1}^{E} w_i = 1$ for each sample. Using the per-sample weights w_i, the mixed distribution parameters for the configuration layer are computed by adding the shared expert output and the weighted sum of fine experts:

$$\mu^{\text{config}}(s) = \mu_{\text{shared}}^{\text{config}}(s) + \sum_{i=1}^{n_{\text{fine}}} w_i^{\text{config}}(s) \mu_i^{\text{config}}(s), \tag{10}$$

$$\log \sigma^{\text{config}}(s) = \log \sigma_{\text{shared}}^{\text{config}}(s) + \sum_{i=1}^{n_{\text{fine}}} w_i^{\text{config}}(s) \log \sigma_i^{\text{config}}(s). \tag{11}$$

We sample the intermediate configuration action as

$$a_1 = \tanh\left(\mu^{\text{config}}(s) + \sigma^{\text{config}}(s) \cdot \epsilon\right), \quad \epsilon \sim \mathcal{N}(0, I). \tag{12}$$

Here, $a_1 \in \mathbb{R}^{d_{\text{config}}}$ represents the configuration decision.
For the signal control stage, we enrich the state with the intermediate action a_1, forming the augmented input as equation (1). The signal action distribution parameters are computed similarly:

$$\mu^{\text{signal}}(\tilde{s}) = \mu_{\text{shared}}^{\text{signal}}(\tilde{s}) + \sum_{j=1}^{n_{\text{fine}}} w_j^{\text{signal}}(\tilde{s}) \mu_j^{\text{signal}}(\tilde{s}), \tag{13}$$

$$\log \sigma^{\text{signal}}(\tilde{s}) = \log \sigma_{\text{shared}}^{\text{signal}}(\tilde{s}) + \sum_{j=1}^{n_{\text{fine}}} w_j^{\text{signal}}(\tilde{s}) \log \sigma_j^{\text{signal}}(\tilde{s}). \tag{14}$$

We then sample the signal action as

$$a_2 = \tanh\left(\mu^{\text{signal}}(\tilde{s}) + \sigma^{\text{signal}}(\tilde{s}) \cdot \epsilon'\right), \quad \epsilon' \sim \mathcal{N}(0, I). \tag{15}$$

Here, $a_2 \in \mathbb{R}^{d_{\text{signal}}}$ represents the signal action.
The final action vector a is the concatenation of configuration and signal actions as

$$a = \text{scale} \cdot [a_1 \ ; \ a_2] + \text{bias}. \tag{16}$$

3.1.3 Load Balance Consideration

Automatically learned routing strategies may encounter the issue of load imbalance, which manifests two notable defects. Firstly, there is a risk of routing collapse [27]. The router repeatedly selects only a small subset of experts for most tokens, preventing other experts from sufficient training [30]. Secondly, persistent load imbalance prevents fair utilization of all experts, which can lead to unequal convergence rates and wasted model capacity [46].

Diversity loss. To mitigate routing collapse, we introduce a diversity loss that encourages the router to maintain high-entropy routing distributions. This ensures that tokens are spread more evenly across experts rather than collapsing onto a few dominant ones:

$$\bar{H}_{\text{config}} = \frac{1}{B} \sum_{b=1}^{B} \left[-\sum_{i=1}^{E} w_{b,i}^{\text{config}} \log w_{b,i}^{\text{config}} \right], \tag{17}$$

$$\bar{H}_{\text{signal}} = \frac{1}{B} \sum_{b=1}^{B} \left[-\sum_{i=1}^{E} w_{b,i}^{\text{signal}} \log w_{b,i}^{\text{signal}} \right], \tag{18}$$

$$\mathcal{L}_{\text{diversity}} = -\left(\bar{H}_{\text{config}} + \bar{H}_{\text{signal}}\right), \tag{19}$$

where B represents the batch size, E represents the number of experts in a router and $w_{b,i}^{\text{config}}$ is normalized routing weight of configuration layer MoDE for sample b and expert i while $w_{b,i}^{\text{signal}}$ is normalized routing weight of signal layer MoDE for sample b and expert i. This term is minimized when the router assigns weights more evenly within each sample, thus reducing the chance of collapse to one or two experts.

Balance loss. In addition, we define an expert-level balance loss that directly regulates the long-term average usage of experts across a batch. This term penalizes disproportionate routing and promotes equalized expert utilization, as expressed by:

$$\mu_i^{\text{config}} = \frac{1}{B} \sum_{b=1}^{B} w_{b,i}^{\text{config}}, \quad \mu_i^{\text{signal}} = \frac{1}{B} \sum_{b=1}^{B} w_{b,i}^{\text{signal}}, \tag{20}$$

$$\mathcal{L}_{\text{balance}} = \frac{1}{E} \sum_{i=1}^{E} \left(\mu_i^{\text{config}}\right)^2 + \frac{1}{E} \sum_{i=1}^{E} \left(\mu_i^{\text{signal}}\right)^2. \tag{21}$$

This term encourages average usage to be spread across experts. This loss reaches its minimum when all experts are equally utilized on average, i.e., when $\mu_i = \frac{1}{E}$ for every expert.

We combine diversity loss and balance loss into a single expert loss term that softly guides the router towards balanced yet specialized routing, with $\lambda = 10^{-3}$ in our

TABLE 1: Notation and parameter definitions.

Parameter	Type	Meaning
a	Hyperparameter	Base number of experts
b	Hyperparameter	Beamforming segmentation factor
c	Hyperparameter	Position segmentation factor
O	State	Observation dimension
P	Action	Position action dimension
B	Action	Beamforming action dimension
H	Model parameter	Shared hidden size.
$H_{e,p}$	Model parameter	Position expert hidden size
$H_{e,b}$	Model parameter	Beamforming expert hidden size
K_p	Model parameter	Number of position experts
K_b	Model parameter	Number of beamforming experts
H_{router}	Model parameter	Router internal hidden size

experiments, balancing the stronger anti-collapse effect with a softer global balancing term.

$$\mathcal{L}_{\text{expert}} = \underbrace{\mathcal{L}_{\text{diversity}}}_{\text{anti-collapse}} + \lambda \underbrace{\mathcal{L}_{\text{balance}}}_{\text{load equalization}}. \tag{22}$$

3.2 SAC Feedback Framework

SAC is explicitly designed for RL tasks with continuous action spaces, employing entropy-regularized policy optimization to encourage robust exploration. Its off-policy nature further enhances data efficiency by reusing past experience from a replay buffer [47]. These characteristics render SAC particularly suitable for continuous control in dynamic wireless environments, supporting adaptive and sample-efficient policy updates [48].

We therefore adopt SAC as the reinforcement learning backbone, which comprises an actor network and two critic networks. The actor, parameterized by θ, implements the policy $\pi_\theta(s)$ and outputs continuous control actions, while the two critics network Q_ϕ and Q_ψ estimate state-action values independently to mitigate overestimation bias. In our implementation, the actor is realized using the proposed MoDE-based actor network, enabling structured and scalable policy representation. The algorithm leverages a large off-policy replay buffer to store state transitions and perform minibatch-based updates.

Training proceeds over E episodes, each beginning from an initial state s and terminating upon meeting a terminal condition, such as task completion, step limit attainment, or failure. At each step, the actor samples an action a from $\pi_\theta(s)$, and the environment returns a user-centric reward r, typically formulated based on utility metrics. These transitions (s, a, r, s') are stored in the replay buffer and later sampled to update the actor and critics via gradient descent. The critic networks are optimized by minimizing the temporal-difference error between predicted and target Q-values, while the actor is updated to maximize the expected return augmented with policy entropy. This entropy regularization fosters exploration and stabilizes learning in continuous action spaces. Through iterative training across episodes, the policy progressively refines its decision-making capacity, converging toward a robust and effective controller for complex wireless optimization tasks.

3.3 Overall Complexity

We adopt the following notation used throughout the complexity analysis in table 1, where $H_{e,p} = H_{e,b} = H/2$, $K_p = a \cdot c$, and $K_b = a \cdot b$. We analyze complexity in two complementary ways.

Parameter count. Below we give exact layerwise sum expressions for the two main model families considered. (i) The per-Expert Feed-Forward Network (ExpertFFN) described in Sec. 3.1.2 is used in our MoDE-based actor network. (ii) We use a two-layer MLP actor for comparison. As each ExpertFFN consists of two dense internal linear layers plus two output heads including mean and log-std. Denoting the expert input dimension by I, the expert hidden width by H, and the expert output dimension by O, the exact parameter count of a single expert is

$$\begin{aligned}\text{Params}_{\text{expert}}(I, H, O) = &\big(I \cdot H + H\big) \\ &+ \big(H \cdot H + H\big) \\ &+ \big(H \cdot O + O\big) \\ &+ \big(H \cdot O + O\big)\end{aligned}$$

Using the expert formula above, plus exact sums for shared experts and router layers, the dense MoDE parameter total is given by

$$\begin{aligned}\text{Params}_{\text{MoDE}} = &K_p \cdot \text{Params}_{\text{expert}}(O, H_{e,p}, P) \\ &+ K_b \cdot \text{Params}_{\text{expert}}(O + P, H_{e,b}, B) \\ &+ \text{Params}_{\text{shared\_pos}}(O, H, P) \\ &+ \text{Params}_{\text{shared\_bf}}(O + P, H, B) \\ &+ \text{Params}_{\text{routers}}.\end{aligned}$$

Asymptotically the dominant terms are those proportional to H^2 coming from multiple experts as

$$\text{Params}_{\text{MoDE}} = \Theta\big(a \cdot (OH + H(P + B) + H^2(\tfrac{1}{b} + \tfrac{1}{c})) + H^2\big).$$

For the two-layer MLP actor with hidden width H_{MLP}, input dimension O and total action dimension $A = P + B$, the exact parameter count is

$$\begin{aligned}\text{Params}_{\text{MLP}} = &\big(O \cdot H_{\text{MLP}} + H_{\text{MLP}}\big) \\ &+ \big(H_{\text{MLP}} \cdot H_{\text{MLP}} + H_{\text{MLP}}\big) \\ &+ \big(H_{\text{MLP}} \cdot A + A\big) \\ &+ \big(H_{\text{MLP}} \cdot A + A\big).\end{aligned}$$

Asymptotically the parameter count is

$$\text{Params}_{\text{MLP}} = \Theta(H_{\text{MLP}}^2 + H_{\text{MLP}}(O + A)).$$

FLOPs Analysis. We analyze computational complexity using the standard multiply-accumulate operation convention. This count includes the bias terms. Pointwise nonlinearities, e.g., ReLU, are treated as lower-order contributions and omitted from the leading-order analysis.

For the ExpertFFN block comprising two hidden linear layers and two parallel output heads, the FLOPs can be expressed as

$$\text{FLOPs}_{\text{expert}}(\text{in}, H, \text{out}) = 2\big(\text{in} \cdot H + H^2 + 2H \cdot \text{out}\big).$$

As for MoDE, we sum across all expert networks, shared

components, and routing mechanisms as

$$\begin{aligned}\text{FLOPs}_{\text{MoDE}} =& K_p \cdot \text{FLOPs}_{\text{expert}}(O, H_{e,p}, P) \\ &+ K_b \cdot \text{FLOPs}_{\text{expert}}(O+P, H_{e,b}, B) \\ &+ \text{FLOPs}_{\text{shared\_pos}} + \text{FLOPs}_{\text{shared\_bf}} \\ &+ \text{FLOPs}_{\text{routers}} + \text{FLOPs}_{\text{aggregation}},\end{aligned}$$

where the aggregation FLOPs account for the weighted summation of expert outputs including mean and log-std, calculated as $2 \cdot (K_p \cdot P + K_b \cdot B)$.
As for the two-layer MLP, FLOPs are summed as

$$\text{FLOPs}_{\text{MLP}} = 2\big(O \cdot H_{\text{MLP}} + H_{\text{MLP}}^2 + 2H_{\text{MLP}} \cdot A\big).$$

Retaining only the dominant contributions, the quadratic in H, yields the leading-order approximations as

$$\text{Params}_{\text{MoDE}} \approx C_{\text{MoDE}}\, H^2, \qquad \text{Params}_{\text{MLP}} \approx H_{\text{MLP}}^2,$$

with $C_{\text{MoDE}} = a\left(\frac{1}{b} + \frac{1}{c}\right) + \mathcal{O}\left(\frac{O}{H}, \frac{A}{H}\right)$. Using the parameter and FLOP expressions above we can form compact measures of the additional complexity introduced by the MoDE-based actor network. Let

$$R_{\text{params}} \triangleq \frac{\text{Params}_{\text{MoDE}}}{\text{Params}_{\text{MLP}}}, \qquad R_{\text{FLOPs}} \triangleq \frac{\text{FLOPs}_{\text{MoDE}}}{\text{FLOPs}_{\text{MLP}}},$$

so that

$$R_{\text{params}} \approx \frac{C_{\text{MoDE}}\, H^2}{H_{\text{MLP}}^2}, \qquad R_{\text{FLOPs}} \approx \frac{\widetilde{C}_{\text{MoDE}}\, H^2}{H_{\text{MLP}}^2},$$

where $\widetilde{C}_{\text{MoDE}}$ differs from C_{MoDE} by small constants accounting for head sizes and aggregation operations.

Two practical observations follow. First, the relative overhead depends primarily on (i) the base expert multiplier a and the segmentation factors b, c and (ii) the choice of the MoDE shared hidden width H and the MLP hidden width H_{MLP}. If the MLP hidden width is chosen to match the effective representational capacity of the MoDE-based actor network, e.g., $H_{\text{MLP}} \approx \sqrt{C_{\text{MoDE}}}\, H$, then R_{params} and R_{FLOPs} approach unity. In practice, however, MoDE is used precisely to increase representational capacity in a controlled way, so one typically observes $R > 1$ whose magnitude is determined by the chosen expert counts and segmentation schedule. Despite parameter and FLOPs increase, the MoDE is compatible with DRL practice and does not invalidate convergence behavior observed for typical DRL algorithms, which are proved in the experiments of Sec. 4.

4 Cases

In this section we describe the three representative application scenarios and explain how the proposed layered MoDE-based actor network and the SAC backbone can be applied in each case. We perform experiments for the coupled decision-making problem in PASS, MU-MIMO and RIS-aided-MIMO.

4.1 Joint Decision-Making Problem in PASS

In this subsection, we evaluate the proposed MoDE-aided SAC algorithm on the pinching-antenna placement and beamforming decision problem and then show its effectiveness.

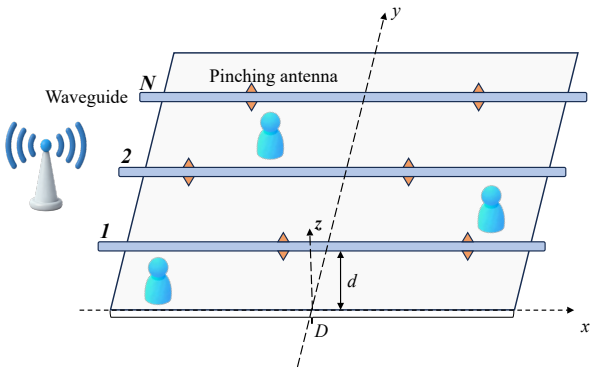

Fig. 2: PASS system model

4.1.1 User-Centric SE Maximization Problem

We consider a downlink multi-user scenario as Fig. 2 with N parallel waveguides at the Base Station (BS) and K single-antenna users deployed in a square region of side length D. Each waveguide carries M pinching antennas positioned along its length; the x-coordinate of the m-th antenna on waveguide n is denoted $x_{m,n}^p \in [0, D]$ and the waveguide height is d.

The objective is user-centric, aiming to maximize an aggregate utility of the instantaneous per-user SE. Let $R_k(s, a)$ denote the instantaneous SE of user k under state s and action a. The optimization objective at each decision step is $\max \sum_{k=1}^K R_k(s, a)$.

The physical propagation model used in the environment follows the structure in PASS. The complex channel from all pinching antennas to user k is collected in the row vector $\mathbf{h}_k^H \in \mathbb{C}^{1\times NM}$, whose entries are small-scale line-of-sight gains. For the m-th antenna on waveguide n the entry is

$$h_{n,m,k} = \frac{\sqrt{\eta}\, \exp\big(-j\frac{2\pi}{\lambda}\|\psi_k - \psi_{m,n}^p\|\big)}{\|\psi_k - \psi_{m,n}^p\|},$$

where $\psi_k = (x_k, y_k, 0)$ is the user location, $\psi_{m,n}^p = (x_{m,n}^p, y_n^p, d)$ is the antenna location, $\lambda = \frac{c}{f_c}$ is the free-space wavelength, and $\eta = \frac{c}{2\pi f_c}$ is the propagation constant used in our implementation. The feed-point phase shifts along each waveguide are collected into a per-waveguide vector $\mathbf{g}_n$, and the block-diagonal pinching matrix $\mathbf{G} = \text{blockdiag}(\mathbf{g}_1, \ldots, \mathbf{g}_N)$ captures the per-antenna phase reweighting induced by the waveguide feed and the specific pinching positions.

Given a baseband precoder matrix $\mathbf{W} = [\mathbf{w}_1, \ldots, \mathbf{w}_K] \in \mathbb{C}^{NM\times K}$ and transmitted symbols x_k, the signal transmitted toward user k is $\mathbf{s}_k = \mathbf{G}\,\mathbf{w}_k\, x_k$. The received scalar signal at user k is therefore

$$y_k = \mathbf{h}_k^H \mathbf{s}_k + \sum_{j\neq k} \mathbf{h}_k^H \mathbf{s}_j + n_k, \tag{23}$$

where $n_k \sim \mathcal{CN}(0, \sigma_0^2)$ is complex Gaussian noise with variance σ_0^2. From this model the instantaneous SINR for user k is

$$\text{SINR}_k(\Phi^p, \mathbf{W}) = \frac{|\mathbf{h}_k^H \mathbf{G}\mathbf{w}_k|^2}{\sum_{j\neq k} |\mathbf{h}_k^H \mathbf{G}\mathbf{w}_j|^2 + \sigma_0^2}, \tag{24}$$

and the per-user SE is

$$R_k(\Phi^p, \mathbf{W}) = \log_2\left(1 + \mathrm{SINR}_k(\Phi^p, \mathbf{W})\right). \tag{25}$$

The learning objective is to maximize an aggregate user utility based on the instantaneous SE. The per-step SE is written as

$$\mathrm{SE}_t = \sum_{k=1}^{K} R_k(\Phi_t^p, \mathbf{W}_t). \tag{26}$$

4.1.2 Beamforming Design

The beamforming latent produced by the actor, denoted $z_w \in \mathbb{R}^L$, is decoded by a small parametric PowerAllocator network into two sets of parameters, a per-user positive uplink factor vector $\boldsymbol{\lambda} = [\lambda_1, \ldots, \lambda_K]^\mathsf{T}$ and a normalized downlink power fraction vector $\mathbf{p} = [p_1, \ldots, p_K]^\mathsf{T}$ with $\sum_k p_k = 1$. In the implementation the mapping is

$$\boldsymbol{\lambda} = \mathrm{softplus}\big(f_\theta(z_w)\big) + \epsilon, \quad \mathbf{p} = \mathrm{softmax}\big(g_\theta(z_w)\big), \tag{27}$$

where f_θ and g_θ are the linear heads of the PowerAllocator network and $\epsilon > 0$ is a small constant for numerical stability. The PowerAllocator architecture and activation choices match the implementation in the environment.

Given the equivalent channel $\widetilde{\mathbf{H}} = \mathbf{H}\mathbf{G} \in \mathbb{C}^{K \times NM}$ that already incorporates the pinching-phase matrix $\mathbf{G}$, the implemented precoder follows a regularized linear structure

$$\mathbf{W} = \widetilde{\mathbf{H}}^\mathsf{H}\Big(\Lambda\, \widetilde{\mathbf{H}}\, \widetilde{\mathbf{H}}^\mathsf{H} + \sigma^2 \mathbf{I}_K\Big)^{-1} \mathbf{P}^{1/2}, \tag{28}$$

where $\Lambda = \mathrm{diag}(\boldsymbol{\lambda})$ and $\mathbf{P}^{1/2} = \mathrm{diag}(\sqrt{p_1}, \ldots, \sqrt{p_K})$. The inverse is implemented as a direct matrix inverse with fallback to a pseudo-inverse when necessary to avoid numerical singularities. Finally, $\mathbf{W}$ is normalized by its Frobenius norm to satisfy the total transmit-power constraint as

$$\mathbf{W}' = \frac{\mathbf{W}}{\|\mathbf{W}\|_F}. \tag{29}$$

With $\mathbf{W}$ and $\widetilde{\mathbf{H}}$ computed, we evaluate the SINR of each user using equation (24), in the implementation the term $\mathbf{G}\mathbf{w}_k$ is replaced by the corresponding columns of $\widetilde{\mathbf{H}}^\mathsf{H}\mathbf{W}$.

4.1.3 MoDE-Aided SAC for PASS Optimization

To address the non-convex challenge outlined in Sec. 2, we design a MoDE-based actor network composed of two sequential stages. The first stage proposes pinching positions for the antennas, and the second produces beamforming latent codes. Below we detail the SAC state space, action space, and reward function:

- **State** s: The state is designed to include the environment and configuration variables relevant to antenna placement and beamforming. Concretely, the state contains user positions, current pinching positions, and the complex channel matrix represented by its real and imaginary parts. We therefore write the state space as

$$\mathcal{S} = \{\{\mathbf{k}_i\}, \{\mathbf{p}_i\}, \{r_i\}\}, \tag{30}$$

  where user positions, stacked as $(x_1, y_1, \ldots, x_K, y_K)$, length $2K$; current pinching positions flattened over waveguides and antennas, length NM; the complex channel state $\mathbf{H}$ represented by its real and imaginary parts and flattened to length $2KMN$.

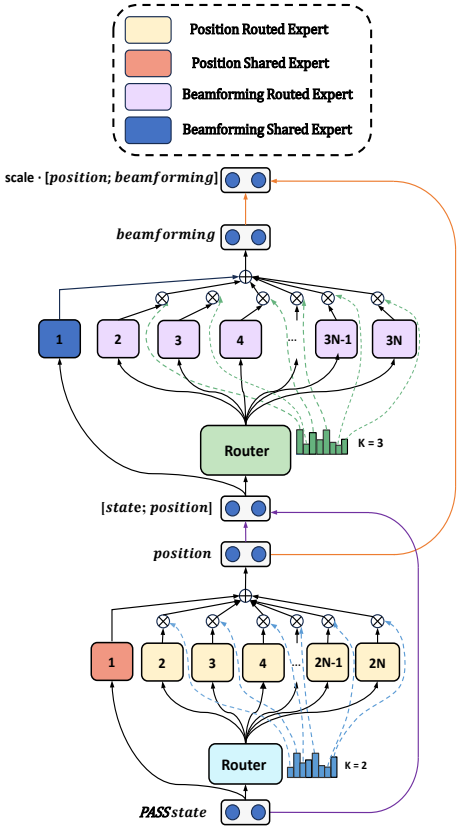

Fig. 3: Illustration of MoDE in PASS.

- **Action** a: The action space A is defined as the optimization process of PAs-position together with beamforming matrics W, which concatenates normalized initial per-waveguide positions, relative inter-antenna increments, and the beamforming latent vector z_w. The continuous action $a_t \in \mathbb{R}^A$ is partitioned as

$$a_t = \left[\mathbf{x}_1^{(n)},\ \Delta^{(n,m)},\ z_w\right],$$

  where $\mathbf{x}_1^{(n)} \in \mathbb{R}^N$ contains normalized first-antenna positions per waveguide, constrained to the range $[-1, 1]$ and mapped to physical coordinates by $x_{1,n}^p = (x_{1,n}^{(n)} + 1)\, D/2$; $\Delta^{(n,m)} \in \mathbb{R}^{N(M-1)}$ are normalized relative increments for subsequent antennas on each waveguide; each normalized delta is mapped to a feasible incremental distance that enforces the minimum spacing $\Delta_{\min}$ and ensures the last antenna remains within $[0, D]$; $z_w \in \mathbb{R}^L$ is the beamforming latent vector decoded by a small PowerAllocator network into per-user uplink factors $\{\lambda_k\} > 0$ and normalized downlink power fractions $\{p_k\}$ with $\sum_k p_k = 1$.
- **Reward** r: The reward function takes into account the objective function, the sum SE. It is designed as aggregating per-user utilities and used for training and evaluation in the environment implementation, we take the per-episode step reward to be propor-

tional to the sum SE with a small improvement bonus, namely

$$r_t = 10\Big(\mathrm{SE}_t + 0.1\big(\mathrm{SE}_t - \mathrm{SE}_{t-1}\big)\Big), \qquad (31)$$

where SE_t is defined in equation (26) and SE_{t-1} denotes the previous step value; the increment term is omitted at the first step; the multiplicative factor is a numeric scaling chosen for training stability.

4.1.4 Concrete Numeric Example Using PASS Case

We now instantiate the algebraic expressions for the PASS environment used in the experiments with $N = 3$ waveguides, $M = 2$ pinching antennas per waveguide, and $K = 6$ users, which gives the following dimensions $O = 90, P = 6, B = 16, A = 22$. We set the model hyperparameters as $H = 256, H_{MLP} = 512, a = 2, b = 3, c = 2$.

From the instrumented numbers in Table 2, the MoDE-based actor network uses approximately 5.59×10^5 parameters and 1.11×10^6 forward FLOPs at initialization, while the MLP with $H_{\mathrm{MLP}} = 512$ uses approximately 3.32×10^5 parameters and 6.62×10^5 FLOPs. Thus, for this configuration, MoDE increases both parameter count and forward FLOPs by approximately a factor of

$$\frac{\mathrm{Params}_{\mathrm{MoDE}}}{\mathrm{Params}_{\mathrm{MLP}}} \approx 1.68, \qquad \frac{\mathrm{FLOPs}_{\mathrm{MoDE}}}{\mathrm{FLOPs}_{\mathrm{MLP}}} \approx 1.68.$$

4.1.5 Experimental Results

We consider a PASS case with N waveguides, each equipped with M pinching antennas. A total of K users are uniformly distributed in a $D \times D = 100 \times 100\,\mathrm{m}^2$ square region. The waveguide height is set to $d = 3\,\mathrm{m}$, the carrier frequency is $f_c = 28\,\mathrm{GHz}$, the effective refractive index is $n_{\mathrm{eff}} = 1.4$, and minimum inter-antenna spacing is $\Delta_{\min} = \lambda_g$. Without loss of generality, We consider multiple training scenarios to demonstrate robustness across system sizes.

Fig. 4 plots the cumulative episodic return versus training iterations for MoDE with SAC, MLP with SAC and a deterministic baseline under identical random seeds and hyperparameters.. In the baseline, the first antenna on each waveguide is aligned with the nearest user in the x-direction, the remaining antennas are placed at the minimum spacing, and the transmit beamforming is implemented using Zero-Forcing (ZF). It shows the scenario where N = 2, M = 2 and K = 4 and the scenario using N = 7, M = 3 and K = 13. In both scenarios, MoDE-aided SAC attains higher final episodic return than MLP-aided SAC and it surpasses the deterministic baseline after sufficient training.

Fig. 5 focuses on the effect of expert allocation across the two MoDE layers and displays the learning curves for these two allocations together with the deterministic baseline. It uses N = 3, M = 2 and K = 6. Here we fix the basic expert count to 3 and compare two layerwise allocations. Configuration A uses fine grained segmentation factor 1 for the position layer and factor 4 for the beamforming layer, which yields 3 experts for the position stage and 12 fine grained experts for the beamforming stage. Configuration B uses segmentation factor 2 for both layers, which yields 6 experts in each layer. The results show that allocating more experts to the beamforming layer produces higher converged episodic return than the symmetric allocation. The symmetric allocation still improves slightly upon the deterministic baseline, but it is outperformed by the beamforming heavy configuration.

Fig. 6 plots the late-training average episodic return as a function of number of experts for three methods including MoDE with SAC, MLP with SAC, and a heuristic baseline. The total expert count combines the base expert number with the fine-grained segmentation factors used in our MoDE-based actor network. Results are reported for two environment configurations including a higher-complexity setting with $N = 5, M = 3, K = 10$ and a lower-complexity setting with $N = 3, M = 2, K = 6$.

TABLE 2: Comparison of concrete complexity for the PASS case using MoDE and MLP actor.

Component	Parameters	Forward FLOPs (approx)
MoDE-based actor network		
Position expert (per)	29,708	—
Position experts (total)	118,832	—
Beamforming expert (per)	33,056	—
Beamforming experts (total)	198,336	—
Shared position expert	92,172	—
Shared beamforming expert	98,848	—
Routers (pos / bf)	24,324 / 26,374	—
MoDE total	**558,886**	**1,109,232**
Baseline MLP actor		
MLP: fc1 (O → H), fc2 (H → H)	46,592 / 262,656	—
MLP: mean / logstd heads	11,286 / 11,286	—
MLP total (H=512)	**331,820**	**661,504**

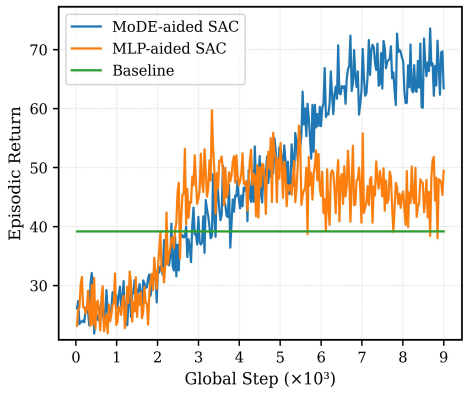

(a) N = 2, M = 2, K =4

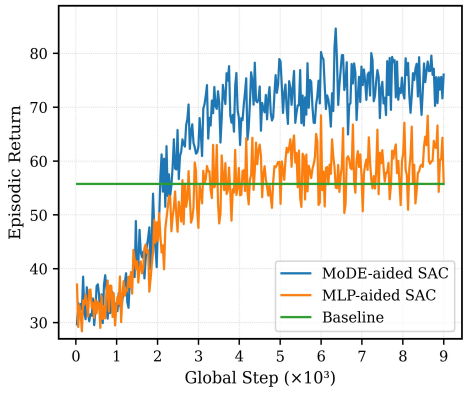

(b) N = 7, M = 3, K =13

Fig. 4: Comparison of average return versus training steps for MoDE–aided SAC, MLP-aided SAC and the heuristic baseline in PASS.

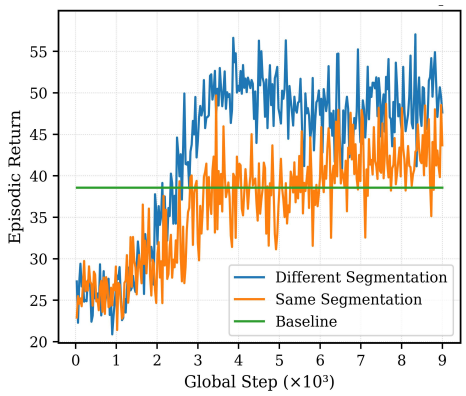

Fig. 5: Average return versus training steps for MoDE with different configuration of experts.

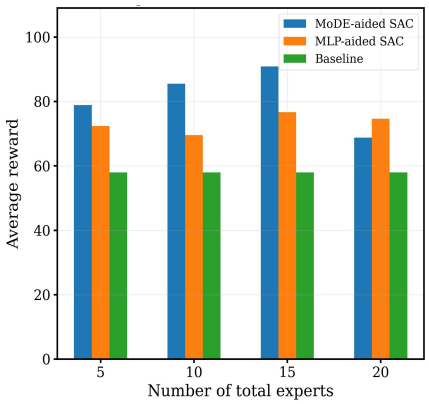

(a) N = 5, M = 3, K = 10

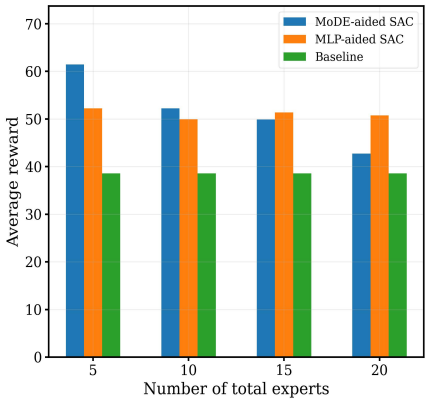

(b) N = 3, M = 2, K = 6

Fig. 6: Impact of total expert count on late-stage episodic return under different environment complexities.

In the higher-complexity environment MoDE improves as the expert count increases up to an intermediate optimum, after which performance degrades. This pattern indicates that in a complex environment additional experts provide useful representational capacity and specialization up to a point. However, more experts also increase routing complexity and decrease the effective per-expert sample size, which amplifies optimization variance, leading to increased noise in parameter updates. Therefore experts can be underutilised or poorly trained , resulting harm performance. Conversely, in the lower-complexity environment, increasing the number of experts tends to decrease MoDE performance. This shows that when the task complexity is low, an overly large expert pool increases optimization difficulty and leads to worse late-stage performance.
Consequently there is a modality-dependent optimum. Moderate expert counts are preferred for complex environments while smaller expert pools are preferable for simpler environments.

Fig. 7 visualizes the gating activations produced by the MoDE-based actor network under the PASS environment with $N = 3$, $M = 2$, and $K = 6$. We set a basic expert number count of 2, position segmentation of 2, and the beamforming sementation of 3. Each heatmap cell shows the router output probability for a single expert, taking values in $[0, 1]$. Rows 1 to 4 correspond to the position experts and rows 5 to 10 correspond to the beamforming experts. Columns 1 to 4 correspond to four environment groups, including variations such as different user-position configurations and different SNR settings.
Panels (a)/(c) show activations at an early stage, while panels (b)/(d) show activations at a later stage after training. Panels (a)/(b) showcase the gating activation in different user position settings. Initially the routing strongly privileges 'pos3' for several user-position groups, reflecting an early bias toward a single positional expert. After training the distribution of position activations becomes more balanced for many groups, while beamforming experts develop distinct fingerprints across user sets. For instance, user-position set 2 after training shows relatively larger contributions from 'bf5' and 'bf6', while in user-positioin set 4 the gating activation is nearly equal, which demonstrates that beamforming experts have specialized to serve different spatial interference patterns produced by distinct user layouts. Panels (c)/(d) showcase the router activation in different SNR settings. At the early stage, the router biases are largely stationary across SNR groups. The position expert 'pos3' has the largest share ≈ 0.287 and the beamforming expert 'bf5' is also relatively large ≈ 0.236 in every column, indicating a weak dependence on SNR at this stage. After training, the router becomes more context-sensitive, that is, the position experts are more evenly utilized across SNR groups, while beamforming allocations vary with the SNR group. For example, 'bf5' is notably higher for SNR = 80 group, and 'bf1' shows larger contributions in SNR = 90 group. This change indicates that training induces specialization in the beamforming experts according to channel conditions, while position experts provide a relatively uniform positional encoding.
Taken together, the results demonstrate two main points. First, the MoDE router achieves adaptive, interpretable gating by learning to adapt expert selection to environmental context. Training shifts router output from a near-single-expert bias toward a richer, instance-dependent allocation, which illustrates the emergence of task-dependent expert specialization. Second, the MoDE structure yields functional specialization. Position experts encode coarse spatial decisions since they become more evenly engaged after training, while beamforming experts specialize to subtle differences between environment such as channel/SNR conditions and

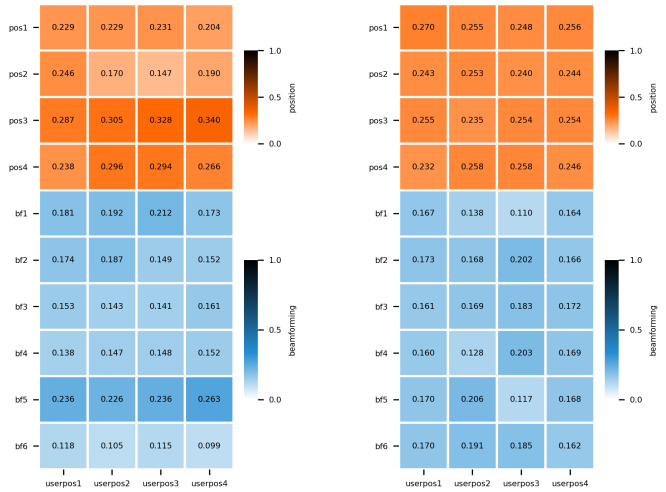

(a) Gating activations before training across user position groups

(b) Gating activations after training across user position groups

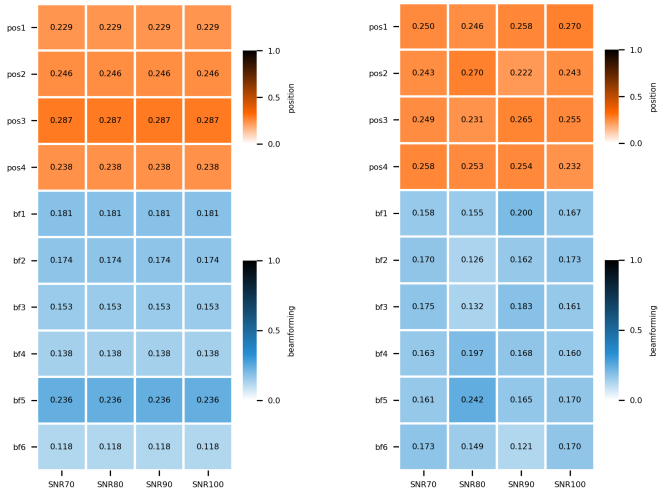

(c) Gating activations before training across SNR groups

(d) Gating activations after training across SNR groups

Fig. 7: Gating activations across environment settings of user-position and SNR variations.

user-position sets. By letting different experts focus on distinct sub-problems, the actor can represent more complex, context-dependent policies without dramatically increasing per-step decision complexity.

4.2 Joint Decision-Making Problem of Power Allocation and Beamforming Design in MU-MIMO

In this subsection, we show the system model under MU-MIMO and evaluate the proposed MoDE-aided SAC algorithm on the joint power allocation and beamforming decision problem.

4.2.1 MU-MIMO System Model

We consider a downlink multi-user MIMO system as depicted in Fig. 8, where a BS equipped with N transmit antennas serves K single-antenna users uniformly distributed

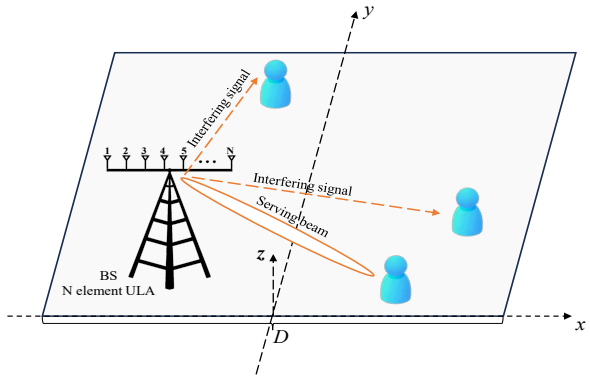

Fig. 8: MU-MIMO system model

in a $D \times D$ square meter area. The received signal at user k is given by

$$y_k = \mathbf{h}_k^H \mathbf{w}_k s_k + \sum_{j \neq k} \mathbf{h}_k^H \mathbf{w}_j s_j + n_k, \tag{32}$$

where $\mathbf{h}_k \in \mathbb{C}^N$ denotes the channel vector from the transmitter to user k, $\mathbf{w}_k \in \mathbb{C}^N$ is the beamforming vector applied to user k, s_k is the unit-power transmitted symbol with $\mathbb{E}[|s_k|^2] = 1$, and $n_k \sim \mathcal{CN}(0, \sigma_k^2)$ is circular complex Gaussian noise. The aggregate channel matrix is defined as $\mathbf{H} = [\mathbf{h}_1, \ldots, \mathbf{h}_K]$ and the channel vector $\mathbf{h}_k$ follows a deterministic LoS model comprising large-scale pathloss, distance-dependent phase delay, and array steering response as

$$\mathbf{h}_k = \sqrt{N\,\rho_k}\ \exp\Big(-j\frac{2\pi}{\lambda}\,\mathrm{dist}_k\Big)\ \overline{\mathbf{a}(\theta_k)},$$

where ρ_k denotes the distance-dependent pathloss, θ_k is the user bearing relative to the array, $\mathbf{a}(\theta)$ is the normalized array response vector, and the overline indicates complex conjugation.

The beamforming design used in this work follows the method described in Sec. 4.1.2, where a key distinction between the MU-MIMO and PASS models is the absence of pinching-induced phase matrix $\mathbf{G}$ in MU-MIMO. Instead, the equivalent channel is the direct physical channel $\mathbf{H}$.

The network utility maximization objective focuses on SE, which is computed from the SINR. We first decompose each beamformer into power and normalized direction components as $\mathbf{w}_k = \sqrt{p_k}\,\mathbf{v}_k$, with $p_k \geq 0$ and $\|\mathbf{v}_k\| = 1$. Hence, the SINR for user k is then expressed as

$$\mathrm{SINR}_k(\{p_j, \mathbf{v}_j\}) = \frac{p_k \left|\mathbf{h}_k^H \mathbf{v}_k\right|^2}{\sum_{j \neq k} p_j \left|\mathbf{h}_k^H \mathbf{v}_j\right|^2 + \sigma_k^2}, \tag{33}$$

and the total SE becomes $\mathrm{SE} = \sum_{k=1}^{K} \log_2\left(1 + \mathrm{SINR}_k\right)$. The optimization objective is to maximize this SE metric.

4.2.2 MoDE-Aided SAC for MU-MIMO Optimization

The MoDE architecture for MU-MIMO, illustrated in Fig. 9, employs a layered expert structure to handle the coupled nature of power allocation and beamforming design. The first layer processes the MU-MIMO system state through

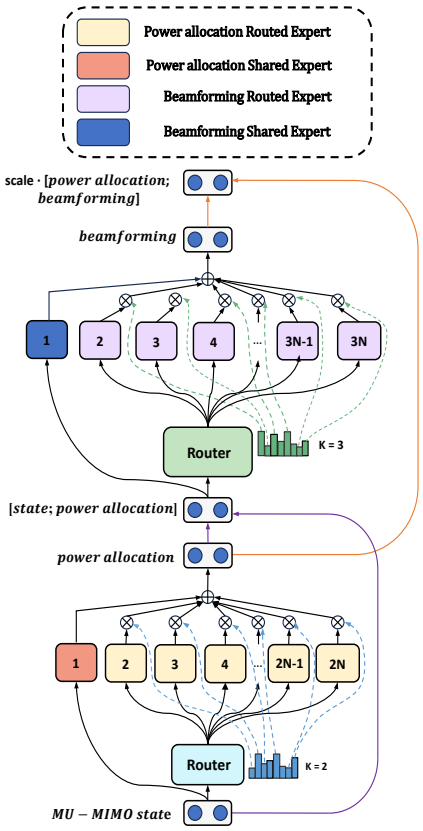

Fig. 9: Illustration of MoDE in MU-MIMO.

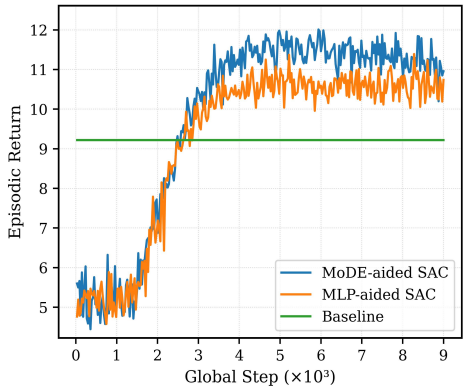

(a) N = 11, K = 18, D = 40

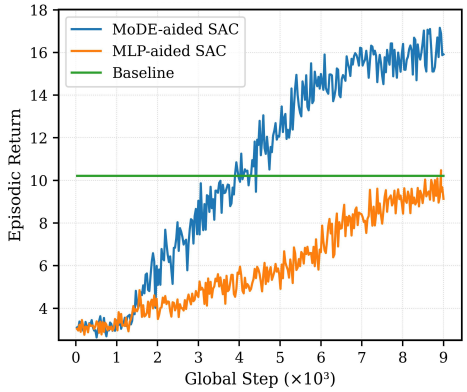

(b) N = 7, K = 13, D = 50

Fig. 10: Comparison of average return versus training steps for MoDE–aided SAC, MLP-aided SAC and the heuristic baseline in MU-MIMO.

configuration experts that output user power allocation factors of dimension K. The second layer concatenates the original system state, forming an augmented input that is routed to siganl experts. These experts produce latent representations of dimension 24 for precoding optimization. The complete action vector a combines both the power allocation factors and beamforming latent vectors, enabling coordinated decision-making.

In our SAC implementation, the state encompasses current channel measurements $\mathbf{H}$, user geographical positions, and antenna array geometry. The continuous action vector encodes both power allocation and beamforming parameters, maintaining end-to-end differentiability. The reward function directly corresponds to the objective in equation (31), with entropy regularization in SAC encouraging exploration across diverse configuration-beamforming combinations and enhancing robustness in multimodal optimization landscapes.

4.2.3 Experimental Results

We evaluate the proposed MoDE-aided SAC on the joint power allocation and beamforming optimization task in MU-MIMO systems. The system operates at a carrier frequency of $f_c = 28$ GHz with a path loss exponent of 2.5. We consider different training scenarios to demonstrate robustness across different system configurations.

Fig. 10 presents the average return versus training steps for MoDE with SAC, MLP with SAC , and a heuristic baseline under identical random seeds and hyperparameters. The baseline employs MMSE precoding combined with water-filling power allocation. The results show when $N = 7$, $K = 13$, $D = 50$ and when $N = 11$, $K = 18$, $D = 40$, MoDE-aided SAC demonstrates faster convergence speed and achieves a higher final performance compared to MLP-aided SAC, with both significantly outperforming the baseline after sufficient training.

4.3 Joint Decision-Making Problem of RIS Phase and Beamforming Design in RIS-Aided MIMO

This subsection presents the RIS-aided MIMO system model and evaluates the proposed MoDE-aided SAC algorithm for the joint optimization of RIS phase shifts and beamforming design.

4.3.1 RIS-Aided MIMO System Model

We consider a RIS-aided MIMO downlink as illustrated in Fig. 11, where a BS equipped with M transmit antennas serves K single-antenna users uniformly distributed in a $D \times D\,\mathrm{m}^2$ square region, through both direct links and reflections from a RIS comprising N passive elements. The channel components include $\mathbf{G} \in \mathbb{C}^{N\times M}$ for the BS-to-RIS link, $\mathbf{r}_k \in \mathbb{C}^{N\times 1}$ for the RIS-to-user k link, and $\mathbf{d}_k \in \mathbb{C}^{M\times 1}$ for the direct BS-to-user k link. The RIS reflection behavior is characterized by the diagonal phase shift matrix $\Theta = \mathrm{diag}(e^{j\theta_1}, \ldots, e^{j\theta_N})$, which enables dynamic manipulation of the propagation environment. Therefore, the composite

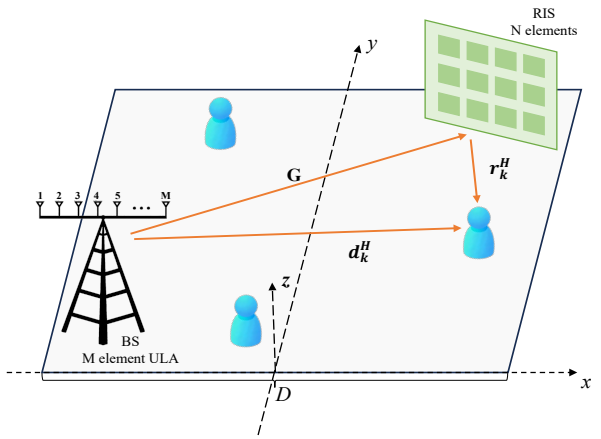

Fig. 11: RIS-aided-MIMO system model

channel response for user k, incorporating both reflected and direct paths, is given by

$$\mathbf{h}_k^H = \mathbf{r}_k^H \mathbf{\Phi} \mathbf{G} + \mathbf{d}_k^H, \tag{34}$$

with the overall effective channel matrix $\mathbf{H} \in \mathbb{C}^{K \times M}$ constructed from rows $\mathbf{h}_k^H(\Theta)$. Given a transmit precoder $\mathbf{W} = [\mathbf{w}_1, \ldots, \mathbf{w}_K] \in \mathbb{C}^{M \times K}$ and unit-power transmitted symbols s_j, the received signal at user k can be expressed as

$$y_k = \mathbf{h}_k^H(\Theta) \sum_{j=1}^{K} \mathbf{w}_j s_j + n_k, \tag{35}$$

with $n_k \sim \mathcal{CN}(0, \sigma_k^2)$ representing the additive noise. Our objective is to maximize a network utility function defined over instantaneous user rates and the system performance is quantified through the SINR for each user as

$$\mathrm{SINR}_k(\Theta, \mathbf{W}) = \frac{\left|\mathbf{h}_k^H(\Theta)\, \mathbf{w}_k\right|^2}{\sum_{j \neq k} \left|\mathbf{h}_k^H(\Theta)\, \mathbf{w}_j\right|^2 + \sigma_k^2}. \tag{36}$$

And the total SE objective is evaluated in the usual way as $\mathrm{SE} = \sum_{k=1}^{K} \log_2\left(1 + \mathrm{SINR}_k(\Theta, \mathbf{W})\right)$.

Our beamforming implementation builds upon the framework established in Sec. 4.1.2, with the distinctive feature that RIS-aided MIMO utilizes the effective channel $\mathbf{H}(\Theta)$ directly without the pinching-phase matrix $\mathbf{G}$ present in other configurations. The precoding matrix $\mathbf{W}$ is normalized to satisfy total transmit power constraints while maximizing SE.

4.3.2 MoDE-Aided SAC for RIS-Aided-MIMO Optimization

The structure of MoDE in RIS-aided MIMO is depicted in 12. To handle the heterogeneous nature of RIS phase adjustments and beamforming design, the actor employs a layered mixture of experts architecture. The first layer processes the RIS-aided MIMO system state through configuration experts that generate RIS phase configurations, outputting both sine and cosine components of phase shifts with dimension $2N$. This phase information is then concatenated with the original state representation to form an enriched input for the second expert layer, which specializes in beamforming latent representation generation for precoder

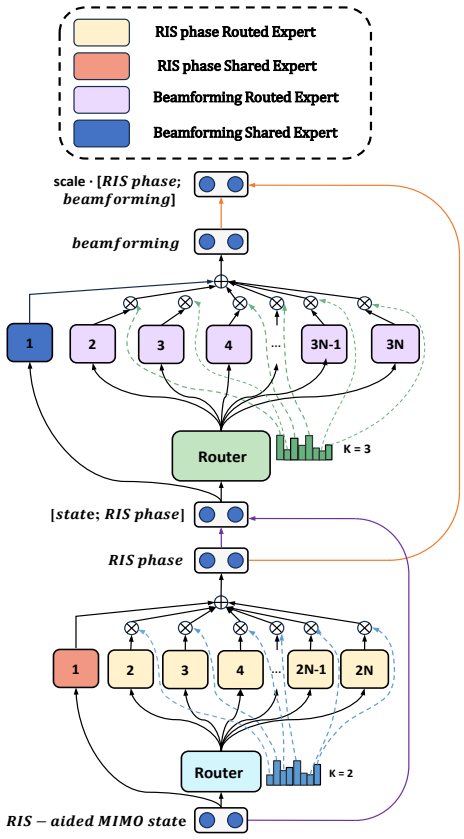

Fig. 12: Illustration of MoDE in RIS-aided MIMO.

optimization. This hierarchical decomposition enables coordinated optimization where RIS phase adjustments establish favorable propagation conditions that the beamforming module subsequently exploits.

In our SAC implementation, the state includes previous RIS phase shifts, current effective channel measurements $\mathbf{H}$, and user positions. The continuous action vector encodes both RIS phase parameters and beamforming latent variables, maintaining full differentiability throughout the optimization pipeline. The reward function directly corresponds to the objective in equation (31), with entropy regularization in SAC promoting exploration across diverse RIS-beamforming configurations and enhancing performance in complex multimodal optimization landscapes.

4.3.3 Experimental Results

We evaluate the proposed MoDE-aided SAC on the joint RIS phase and beamforming optimization task in RIS-aided downlink MISO systems. The system operates at a carrier frequency of $f_c = 3.5$ GHz, region $D = 30$m with path loss exponents of 3.0 for direct links and 2 for RIS-reflected paths. The reference path loss is set to $P_{lo} = -20$ dB at $d_o = 1$ m, with an additional RIS gain of 10 dB enhancing the reflected signals.Two environment configurations are considered to demonstrate robustness across scales.

Fig. 13 present the average return versus training steps for MoDE with SAC, MLP with SAC, and an alternating optimization baseline under identical random seeds and hyperparameters. The baseline operates on local copies of environment channels and alternately updates the MMSE

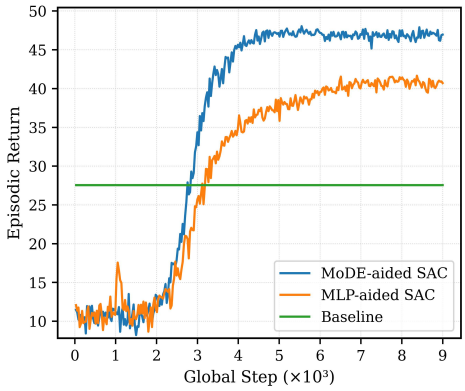

(a) N = 24, M = 2, K = 3

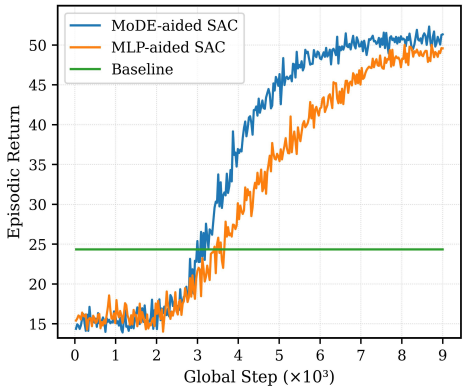

(b) N = 36, M = 4, K = 6

Fig. 13: Comparison of average return versus training steps for MoDE–aided SAC, MLP-aided SAC and the heuristic baseline in RIS-aided MIMO.

precoder and per-element RIS phases via closed-form phase updates. It shows the scenarios with $N = 24$, $M = 2$, $K = 3$, and with $N = 36$, $M = 4$, and $K = 6$. The results show that MoDE-aided SAC demonstrates faster convergence speed and achieves higher final performance compared to MLP-aided SAC. In both configurations, MoDE-aided SAC and MLP-aided SAC significantly outperform the alternating optimization baseline after sufficient training.

5 Conclusion

We proposed a novel approach to enhancing system performance in next-generation wireless networks, focusing on joint physical-layer configuration and resource allocation. Our primary contribution is the MoDE-aided SAC algorithm, designed to address the tightly coupled optimization challenges in high-dimensional, non-convex decision spaces. The framework leverages real-time, sample-efficient feedback on spectral efficiency to enable coordinated adaptation of both system configuration and signal parameters. This capability is validated across three representative scenarios, PASS, MU-MIMO, and RIS-aided MIMO, demonstrating effective joint optimization in each case. Furthermore, the proposed architecture naturally extends to other coupled wireless problems where the layered MoDE assigns specialized experts to complementary subtasks. Overall, our methodology highlights the potential of combining MoDE architectures with DRL to enhance adaptive resource allocation, paving the way for real-time resource management in large-scale 6G wireless networks.

References

[1] H. F. Alhashimi, M. N. Hindia, K. Dimyati, E. B. Hanafi, N. Safie, F. Qamar, K. Azrin, and Q. N. Nguyen, "A survey on resource management for 6g heterogeneous networks: current research, future trends, and challenges," *Electronics*, vol. 12, no. 3, p. 647, 2023.

[2] W. Saad, M. Bennis, and M. Chen, "A vision of 6g wireless systems: Applications, trends, technologies, and open research problems," *IEEE network*, vol. 34, no. 3, pp. 134–142, 2019.

[3] S. Andreev, V. Petrov, M. Dohler, and H. Yanikomeroglu, "Future of ultra-dense networks beyond 5g: Harnessing heterogeneous moving cells," *IEEE Communications Magazine*, vol. 57, no. 6, pp. 86–92, 2019.

[4] R. J. Mailloux, *Phased array antenna handbook*. Artech house, 2017.

[5] Q. Wu and R. Zhang, "Intelligent reflecting surface enhanced wireless network via joint active and passive beamforming," *IEEE transactions on wireless communications*, vol. 18, no. 11, pp. 5394–5409, 2019.

[6] Y. Zeng, R. Zhang, and T. J. Lim, "Wireless communications with unmanned aerial vehicles: Opportunities and challenges," *IEEE Communications magazine*, vol. 54, no. 5, pp. 36–42, 2016.

[7] Y. Mao, C. You, J. Zhang, K. Huang, and K. B. Letaief, "A survey on mobile edge computing: The communication perspective," *IEEE communications surveys & tutorials*, vol. 19, no. 4, pp. 2322–2358, 2017.

[8] F. Guo, F. R. Yu, H. Zhang, X. Li, H. Ji, and V. C. Leung, "Enabling massive iot toward 6g: A comprehensive survey," *IEEE Internet of Things Journal*, vol. 8, no. 15, pp. 11 891–11 915, 2021.

[9] M. Singh and G. Baranwal, "Quality of service (qos) in internet of things," in *2018 3rd International Conference On Internet of Things: Smart Innovation and Usages (IoT-SIU)*. IEEE, 2018, pp. 1–6.

[10] Y. Chen, S. Zhang, S. Xu, and G. Y. Li, "Fundamental trade-offs on green wireless networks," *IEEE Communications Magazine*, vol. 49, no. 6, pp. 30–37, 2011.

[11] Y.-F. Liu, T.-H. Chang, M. Hong, Z. Wu, A. M.-C. So, E. A. Jorswieck, and W. Yu, "A survey of recent advances in optimization methods for wireless communications," *IEEE Journal on Selected Areas in Communications*, 2024.

[12] K. B. Letaief, W. Chen, Y. Shi, J. Zhang, and Y.-J. A. Zhang, "The roadmap to 6g: Ai empowered wireless networks," *IEEE communications magazine*, vol. 57, no. 8, pp. 84–90, 2019.

[13] Z. Feng, Z. Wei, X. Chen, H. Yang, Q. Zhang, and P. Zhang, "Joint communication, sensing, and computation enabled 6g intelligent machine system," *IEEE Network*, vol. 35, no. 6, pp. 34–42, 2022.

[14] Y. Shi, L. Lian, Y. Shi, Z. Wang, Y. Zhou, L. Fu, L. Bai, J. Zhang, and W. Zhang, "Machine learning for large-scale optimization in 6g wireless networks," *IEEE Communications Surveys & Tutorials*, vol. 25, no. 4, pp. 2088–2132, 2023.

[15] X. Xie, F. Fang, and Z. Ding, "Joint optimization of beamforming, phase-shifting and power allocation in a multi-cluster irs-noma network," *IEEE Transactions on Vehicular Technology*, vol. 70, no. 8, pp. 7705–7717, 2021.

[16] M. S. Elbamby, C. Perfecto, C.-F. Liu, J. Park, S. Samarakoon, X. Chen, and M. Bennis, "Wireless edge computing with latency and reliability guarantees," *Proceedings of the IEEE*, vol. 107, no. 8, pp. 1717–1737, 2019.

[17] E. Bastug, M. Bennis, M. Médard, and M. Debbah, "Toward interconnected virtual reality: Opportunities, challenges, and enablers," *IEEE Communications Magazine*, vol. 55, no. 6, pp. 110–117, 2017.

[18] Y. Lu, Z. Zhang, and L. Dai, "Hierarchical beam training for extremely large-scale mimo: From far-field to near-field," *IEEE Transactions on Communications*, vol. 72, no. 4, pp. 2247–2259, 2023.

[19] K. Shen and W. Yu, "Fractional programming for communication systems—part i: Power control and beamforming," *IEEE Transactions on Signal Processing*, vol. 66, no. 10, pp. 2616–2630, 2018.

[20] K. Shen, W. Yu, L. Zhao, and D. P. Palomar, "Optimization of mimo device-to-device networks via matrix fractional programming: A minorization–maximization approach," *IEEE/ACM Transactions on Networking*, vol. 27, no. 5, pp. 2164–2177, 2019.

[21] N. C. Luong, D. T. Hoang, S. Gong, D. Niyato, P. Wang, Y.-C. Liang, and D. I. Kim, "Applications of deep reinforcement learning in communications and networking: A survey," *IEEE communications surveys & tutorials*, vol. 21, no. 4, pp. 3133–3174, 2019.

[22] F. B. Mismar, B. L. Evans, and A. Alkhateeb, "Deep reinforcement learning for 5g networks: Joint beamforming, power control, and interference coordination," *IEEE Transactions on Communications*, vol. 68, no. 3, pp. 1581–1592, 2019.

[23] D. Kim, M. R. Castellanos, and R. W. Heath, "Deep reinforcement learning for beam management in uav relay mmwave networks," *IEEE Communications Magazine*, vol. 62, no. 10, pp. 104–109, 2024.

[24] H. Borchani, G. Varando, C. Bielza, and P. Larranaga, "A survey on multi-output regression," *Wiley Interdisciplinary Reviews: Data Mining and Knowledge Discovery*, vol. 5, no. 5, pp. 216–233, 2015.

[25] D. Xu, Y. Shi, I. W. Tsang, Y.-S. Ong, C. Gong, and X. Shen, "Survey on multi-output learning," *IEEE transactions on neural networks and learning systems*, vol. 31, no. 7, pp. 2409–2429, 2019.

[26] W. Cai, J. Jiang, F. Wang, J. Tang, S. Kim, and J. Huang, "A survey on mixture of experts in large language models," *IEEE Transactions on Knowledge and Data Engineering*, 2025.

[27] N. Shazeer, A. Mirhoseini, K. Maziarz, A. Davis, Q. Le, G. Hinton, and J. Dean, "Outrageously large neural networks: The sparsely-gated mixture-of-experts layer," *arXiv preprint arXiv:1701.06538*, 2017.

[28] B. Pan, Y. Shen, H. Liu, M. Mishra, G. Zhang, A. Oliva, C. Raffel, and R. Panda, "Dense training, sparse inference: Rethinking training of mixture-of-experts language models," *arXiv preprint arXiv:2404.05567*, 2024.

[29] X. Nie, X. Miao, S. Cao, L. Ma, Q. Liu, J. Xue, Y. Miao, Y. Liu, Z. Yang, and B. Cui, "Evomoe: An evolutional mixture-of-experts training framework via dense-to-sparse gate," *arXiv preprint arXiv:2112.14397*, 2021.

[30] W. Fedus, B. Zoph, and N. Shazeer, "Switch transformers: Scaling to trillion parameter models with simple and efficient sparsity," *Journal of Machine Learning Research*, vol. 23, no. 120, pp. 1–39, 2022.

[31] Y. Zhou, T. Lei, H. Liu, N. Du, Y. Huang, V. Zhao, A. M. Dai, Q. V. Le, J. Laudon *et al.*, "Mixture-of-experts with expert choice routing," *Advances in Neural Information Processing Systems*, vol. 35, pp. 7103–7114, 2022.

[32] Y. Liu, Z. Wang, X. Mu, C. Ouyang, X. Xu, and Z. Ding, "Pinching-antenna systems (pass): Architecture designs, opportunities, and outlook," *arXiv preprint arXiv:2501.18409*, 2025.

[33] Z. Ding, R. Schober, and H. V. Poor, "Flexible-antenna systems: A pinching-antenna perspective," *IEEE Transactions on Communications*, 2025.

[34] X. Xu, X. Mu, Z. Wang, Y. Liu, and A. Nallanathan, "Pinching-antenna systems (pass): Power radiation model and optimal beamforming design," *arXiv preprint arXiv:2505.00218*, 2025.

[35] A. Bereyhi, S. Asaad, C. Ouyang, Z. Ding, and H. V. Poor, "Downlink beamforming with pinching-antenna assisted mimo systems," *arXiv preprint arXiv:2502.01590*, 2025.

[36] Q. Shi, M. Razaviyayn, Z.-Q. Luo, and C. He, "An iteratively weighted mmse approach to distributed sum-utility maximization for a mimo interfering broadcast channel," *IEEE Transactions on Signal Processing*, vol. 59, no. 9, pp. 4331–4340, 2011.

[37] T. Yoo and A. Goldsmith, "On the optimality of multiantenna broadcast scheduling using zero-forcing beamforming," *IEEE Journal on selected areas in communications*, vol. 24, no. 3, pp. 528–541, 2006.

[38] C. Li, X. Wang, L. Yang, and W.-P. Zhu, "A joint source and relay power allocation scheme for a class of mimo relay systems," *IEEE Transactions on Signal Processing*, vol. 57, no. 12, pp. 4852–4860, 2009.

[39] E. Ali, M. Ismail, R. Nordin, and N. F. Abdulah, "Beamforming techniques for massive mimo systems in 5g: overview, classification, and trends for future research," *Frontiers of Information Technology & Electronic Engineering*, vol. 18, no. 6, pp. 753–772, 2017.

[40] F. W. Vook, A. Ghosh, and T. A. Thomas, "Mimo and beamforming solutions for 5g technology," in *2014 IEEE MTT-S International Microwave Symposium (IMS2014)*. IEEE, 2014, pp. 1–4.

[41] P. Wang, J. Fang, X. Yuan, Z. Chen, and H. Li, "Intelligent reflecting surface-assisted millimeter wave communications: Joint active and passive precoding design," *IEEE Transactions on Vehicular Technology*, vol. 69, no. 12, pp. 14 960–14 973, 2020.

[42] H. Xie, J. Xu, and Y.-F. Liu, "Max-min fairness in irs-aided multi-cell miso systems with joint transmit and reflective beamforming," *IEEE Transactions on Wireless Communications*, vol. 20, no. 2, pp. 1379–1393, 2020.

[43] X. Li, J. Fang, F. Gao, and H. Li, "Joint active and passive beamforming for intelligent reflecting surface-assisted massive mimo systems," *arXiv preprint arXiv:1912.00728*, 2019.

[44] C. Huang, A. Zappone, G. C. Alexandropoulos, M. Debbah, and C. Yuen, "Reconfigurable intelligent surfaces for energy efficiency in wireless communication," *IEEE transactions on wireless communications*, vol. 18, no. 8, pp. 4157–4170, 2019.

[45] Q. Wu, S. Zhang, B. Zheng, C. You, and R. Zhang, "Intelligent reflecting surface-aided wireless communications: A tutorial," *IEEE transactions on communications*, vol. 69, no. 5, pp. 3313–3351, 2021.

[46] D. Dai, C. Deng, C. Zhao, R. Xu, H. Gao, D. Chen, J. Li, W. Zeng, X. Yu, Y. Wu *et al.*, "Deepseekmoe: Towards ultimate expert specialization in mixture-of-experts language models," *arXiv preprint arXiv:2401.06066*, 2024.

[47] M. Haklidir and H. Temeltaş, "Guided soft actor critic: A guided deep reinforcement learning approach for partially observable markov decision processes," *IEEE Access*, vol. 9, pp. 159 672–159 683, 2021.

[48] Q. Wang, K. Feng, X. Li, and S. Jin, "Precodernet: Hybrid beamforming for millimeter wave systems with deep reinforcement learning," *IEEE Wireless Communications Letters*, vol. 9, no. 10, pp. 1677–1681, 2020.